VIBRATION ISOLATION SCHEME BASED ON ELECTROMAGNETIC SPRING

Tanatip Mayoon[1], Prissana Thamboon[2,*], Nuttanan Tanasanchai[3], Puripong Suthisopapan[1], and Waranont Anukool[2,3]

Received: December 20, 2021; Revised: May 05, 2022; Accepted: May 07, 2022

Abstract

Sensitive measurements require a vibration isolation system to safeguard against detrimental tremble. Two types of vibration isolation systems - passive and active - are currently implemented. The spring-based passive designs usually accompany with ineffective low-frequency response. Therefore, the active designs, consisting of sensors, feedback control systems, and actuators, are consolidated to improve the total effectiveness of the cancellation performance. In this work, we focus on developing the actuator founded on electromagnetic spring to be incorporated into our compact quantum gravimeter. Each spring-actuated part comprises two repelling Nd magnets positioned face to face inside a solenoid. With this configuration, the spring can also work in the passive mode via repulsive magnetic force. In the active mode, the exerted force is a result of magnetic fields formed by the magnets and the current-controlled solenoid coils. By changing the coil current, the stiffness of the spring can be modified, and thus the displacement can be controlled. Different sizes of magnets are explored, and their force behaviors in passive and active modes are characterized. The implementation scheme of the actuator in the quantum gravimeter is also discussed.

Keywords: **Actuator; electromagnetic spring, magnetic spring; solenoid; magnet; vibration isolation**

Introduction

Effective isolation from external vibration is a critical element in an apparatus of a sensitive instrument. The vibro-isolation platform should be able to safeguard against unwanted floor oscillation from dc to a few hundred hertz. Traditionally, suppression of the vibration can be done by placing an isolated device on a flexible support such as a mechanical spring. A frictional damper can also be added to the spring-based system to dissipate the oscillation within; these elements constitute a common design of passive vibration isolation system (passive-VIS) that requires no power consumption, but merely relies on mechanical properties of the materials. However, the prescribed spring stiffness *k* dictates the resonance of the system where vibrational energy transfer

[1] *Department of Electrical Engineering, Faculty of Engineering, Khon Kaen University, Khon Kaen, 4000, Thailand. Email: mayoon@kkumail.com; mr.puripong@gmail.com*
[2] *Research Center for Quantum Technology, Faculty of Science, Chiang Mai University, Chiang Mai, 50200, Thailand. Email: prissana.t@cmu.ac.th; waranont.a@cmu.ac.th*
[3] *Department of Physics and Materials Science, Faculty of Science, Chiang Mai University, 50200, Thailand. Email: nuttanan_tan@cmu.ac.th; waranont.a@cmu.ac.th*
[*] *Corresponding author*

is undesirably amplified. The resonance frequency usually falls in the low frequency regime, making the passive-VIS less attractive. In contrast, an active-VIS utilizing electromechanical control does not have a region of amplification, thus it can isolate in the low frequency. Through orchestration of motion sensors, feedback control systems, and actuators, the active-VIS generates a counter force to cancel external disturbance. In most scenarios, therefore, the active-VIS is implemented in conjunction with the passive-VIS to improve the total effectiveness of vibration cancellation. At the Research Center of Quantum Technology, Chiang Mai University, we are constructing a compact quantum gravimeter with a ppb-level sensitivity of gravitational-acceleration detection. Displacement of a retro-reflecting mirror, serving as the inertial frame of reference for the free-falling atoms, due to ground vibration can lead to a significant error (Kasevich and Chu, 1992). Combined isolation systems are adopted for active displacement control of the mirror featuring either voice coil (Hensley *et al*., 1999; Schmidt *et al*., 2011) or piezoelectric (Sui *et al*., 2012) as the actuator.

Alternatively, a vibration isolation scheme that can work in both passive and active modes could downsize the system as well as lower the cost, which is desirable for our quantum gravimeter. Exploiting controllable magnetic force is an appealing choice. Permanent magnets are easily attainable in the market and can be arranged in a variety of configurations to suit intended applications (Otake, 2000; Wu *et al*., 2014). Two repulsive magnets facing one another form the simplest magnetic spring, which works in the same way as the passive-VIS in supporting and isolating the payload from external shock (Puppin and Fratello, 2002). Furthermore, magnetic springs can be scaled to work with small payloads or large ones such as an optical table (Robertson *et al*., 2005; Oyelade, 2020; Akshay Kumar and Santhosh, 2021). The ability to alter the stiffness of the magnetic spring with current has made this passive system increasingly attractive to an active control system (Snamina and Habel, 2010; Olaru *et al*., 2017; Bednarek *et al*., 2020; Xu *et al*., 2020). Venturing into electromagnetic spring suggests that we can have a vibration isolation scheme that works both in passive and active modes.

Therefore, in this work, the simplest structure of electromagnetic spring is investigated for its potential use in vibration isolation of a compact quantum gravimeter. In the subsequent sections, we describe how we obtain a characterization of the force behaviors in both passive and active experiments. A simple, low cost design of our electromagnetic springs for isolating the mirror in the gravimeter is then introduced. Excellent versatility and scalability of the electromagnetic spring should widen its range of applications for active displacement control.

Materials and Methods

In this work, we employ a repelling scheme of magnetic spring as shown in Figure 1(a) to support the load. Like magnets are vertically positioned face to face to create the levitated force (F_m) counter-balancing the weight of the load (F_L) at the magnet separation z between the faces of the magnets. The vibration isolation mechanism here will be purely mechanical the same as the spring-based system in which we call the passive mode. In the active mode depicted in Figure 1(b), a solenoid coil (SC) is added to the magnetic spring. The current and its polarity ($I\pm$) supplied to the solenoid can bi-directionally shift the load up or down; this is equivalent to creating the spring with variable stiffness. The exerted force now is the electromagnetic force F_e which is the result of interaction between magnetic fields formed by the magnets and the solenoid. In other words, we can actuate the controllable F_e to compensate the displacement from equilibrium due to undesirable vibration force.

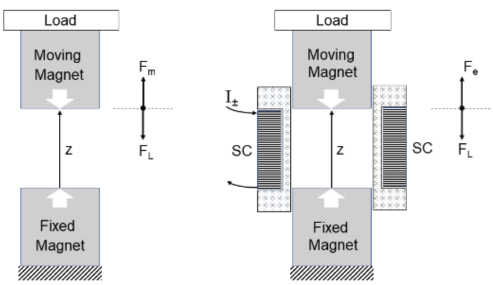

(a) (b)

Figure 1. Schematic diagram of the magnetic spring working on (a) passive-mode and (b) active-mode

Passive-mode Experiment

To explore the force behavior in the passive mode (F_m), we obtained commercially available NdFeB cylindrical magnets of three different sizes, denoted as S, M, and L in Table 1. Resembling Figure 1(a), the lower magnet was held fixed to the base structure made of a 3D printed polylactic acid (PLA) filament, while the upper magnet was attached to the load and free to vertically move to reach a balanced position. Each of the three sizes of fixed magnets was paired up to the same moving magnet size L; thus, we have three pairs of magnetic springs S-L, M-L, and L-L with presumably different stiffness constants to characterize. For a stable vertical movement, we acquired an acrylic pipe of 16-mm diameter to closely confine the magnets; all the magnets, therefore, were resin casted to 15.8 mm in diameter. We then varied the load with known mass, and after the magnetic spring came to rest, we recorded the magnetic force in gram-force of the applied load versus the magnet distance *z*. The magnet distance *z* was measured between faces of the magnet by defining $z = 0$ at the face of the fixed magnet.

Table 1. List of experimental parameters for the passive experiment

Magnet sizes with diameter × length in mm			
Fixed magnet			**Moving magnet**
10×3 (size S)	10×10 (size M)	15×15 (size L)	15×15 (size L)

Table 2. List of experimental parameters for the active experiment

Magnet pair	Solenoid coil	Current
size M - L	13 loops in 4 layers resulting in 15-mm effective length	± 1 to 4 A

Active-mode Experiment

Table 2 summarizes experimental parameters used in the active-mode experiment. The magnet pair M-L was chosen to represent the electromagnetic force behavior (F_e). The solenoid was constructed with a copper wire of 1-mm diameter. The wire was wound into a tight helix around a 3D printed bobbin for 13 rounds in 4 layers, yielding the same length as the moving magnet L of 15 mm. The coil was connected to a current source of 4-A maximum.

By defining $z = 0$ at the face of the fixed magnet shown in Figure 2, the solenoid was positioned between $z = 5$ mm to $z = 20$ mm, covering the acrylic pipe. The value of electromagnetic force versus *z* was obtained differently from the passive-mode experiment. Here the electromagnetic spring was placed on a digital scale (Figure 2), which after resetting to zero displayed the F_e force that is equally against the pressure force from a micrometer. A travel distance of the pressure force read from the micrometer yielded the information of the magnet distance *z*. Since the maximum travel range of the micrometer is 25 mm, the face of the moving magnet was set to shift between $z = 5$ mm to $z = 30$ mm, meaning the moving magnet will be translated from being totally inside the solenoid to being totally outside the solenoid at 10 cm above it. At each distance *z*, the forces with and without current were recorded.

Results and Discussion

Force Behavior in the Passive Mode

The repulsive magnetic forces F_m, plotted in gram-force where 1 gram-force = 0.009807 N, of the three magnet pairs as a function of the magnet distance *z* are shown in Figure 3. All forces exhibit inverse proportion to the magnet separation, i.e., the repulsive magnetic force increases nonlinearly with the decreasing magnet gap. By analogy with the mechanical spring, the deflection rate dF_m/d*z* or the slope of the force curve indicates the stiffness of the magnetic spring. At a certain operating point, the slopes of the magnet pairs S-L, M-L, and L-L increase respectively, meaning the stiffness increases with the magnet dimensions. The high

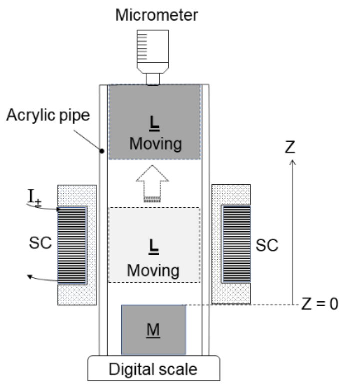

Figure 2. Detailed experimental setup for characterizing the electromagnetic force in the active mode

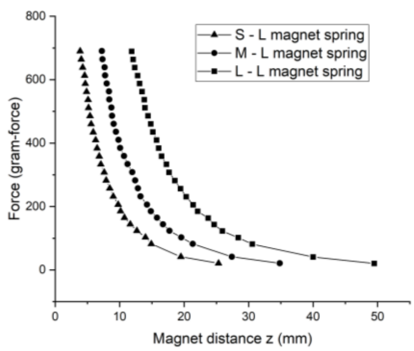

Figure 3. Magnetic forces as a function of magnet distance for the magnet pairs S-L, M-L, and L-L

stiffness magnetic spring can support a wider range of load at the expense of the overall system size as is the case of the L-L magnetic spring.

Unlike the mechanical spring force, the magnetic force exhibits nonlinear nature and thus is more complex. The description of the magnetic force as a function of z can be obtained either using the coulombian approach or the amperian approach; nonetheless, both approaches yield the same end results (Ravaud *et al*., 2010). By means of the coulombian approach, the permanent magnets are treated as magnetic charges governed by the well-known inverse square law of the coulomb force $F(r) \propto 1/r^2$. The exact calculation of magnetic force can be obtained through a numerical method taken also the magnetization and geometry of the magnets into account. For two cylindrical magnets like our system, a good approximation of the force formula can be determined under the assumption that the magnet distance is much larger than the diameter of the magnets. Unfortunately, our magnets all have comparable diameters to the magnet distance. Therefore, we have adapted the coulombian force by assuming multipole expansion to describe the force behavior of our system. Figure 4 displays the experimental force data of the S-L magnets and the two fitted curves. The dashed curve is the one we at first assume the multipole expansion in the form

$$F_m = \sum_{i=2}^{4} \frac{a_i}{z^i} \quad (1)$$

where a_i is the fitting coefficient. It is worth to note that the first term in the multipole expansion is the dipole term. As can be seen from Figure 4, the fitting curve of Equation (1) deviates from the experimental data at small values of magnetic force as the magnets move further apart. This same discrepancy is present in the force data of the M-L magnets, including in the L-L magnets. By adding a linear term to Equation (1), the fitting formula become

$$F_m = \sum_{i=2}^{4} \frac{a_i}{z^i} + kz \quad (2)$$

where k is the fitting coefficient of the linear term, and the fitting result is plotted as a solid curve, which reveals a better fit to the data. This small linear term probably comes from the friction between the moving magnet and the acrylic pipe, which becomes more pronounced as the magnetic force diminishes with increasing z. This could be the damping term of our system.

In Table 3, we list the fitting coefficients in Equation (2) normalized to the dipole term a_2 for all the magnet pairs.

A variety of curve fittings for the magnetic spring force - such as using only the dipole term (Bednarek *et al*., 2020), the Taylor series expansion of odd powers (Olaru *et al*., 2017; Xu *et al*., 2020), or a simple exponential function (Puppin and Fratello, 2002) - is found in the literatures.To further analyze the nonlinear spring system with a well-developed linear control system such as the PID controller, a common practice is to linearize the nonlinear function into the Taylor series where Laplace transform can be applied (Xu *et al*., 2020). However, many real world systems are nonlinear and it is possible to analyze with the nonlinear control system such as the Fuzzy PID controller (Zhang *et al*., 2020). In this work, we simply report the characteristic of our magnetic spring system, which is well-described based on the multipole expansion, and leave further analysis to be the matter of future work.

Force Behavior in the Active Mode

In the active mode, the force exerted by the electromagnetic spring (F_e) is due to the interaction of magnetic fields formed by the magnets and the coils. According to the Lorentz force law, the F_e is bi-directional depending on the direction of the loop current with respect to the magnetic field of the permanent magnets. In our setup, the counterclockwise current supplied by the positive polarity from the current source lifts the load up, while the negative

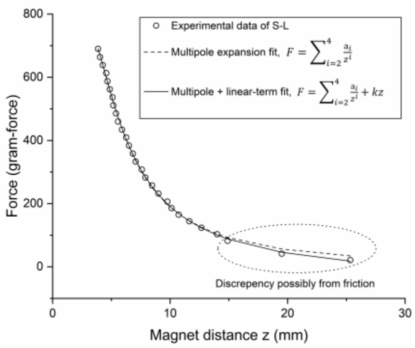

Figure 4. Fitting curves of the magnetic force experimental data. The area circled is where the two fitting curves differ

Table 3. Fitting coefficients normalized to the dipole term a_2

	$F_m = \sum_{i=2}^{4} \frac{a_i}{z^i} + kz$			
	a_2	a_3	a_4	k
S-L	1	-2.77	1.52	-2.9×10^{-5}
M-L	1	-1.37	-4.25	-1.4×10^{-5}
L-L	1	111.65	-814.98	-3.4×10^{-6}

polarity does the opposite. In other words, the positive current effectively increases the stiffness of the magnetic spring F_m. As the distance z is kept fixed by the pressure force, tis results in the increased of electromagnetic force F_e shown in the ratio force curve (Figure 5). For the positive currents ranging from +1A to +4A, we obtain the force ratios F_e/F_m of greater than 1, which is directly proportion to the amount of current. As expected, the negative current of -2A in the graph yields the force ratio of less than 1, which indicates the decrease in magnetic spring stiffness.

Considering closely at the force-ratio curves in the positive current regime, during the first quarter of the solenoid range, the supplied current barely has any effect on the spring stiffness. After that, the force-ratio curves continue to rise to the peak outside the solenoid range before gradually declining (see the extension curve for I = +4A after z = 30 mm). We take a portion of the data between z = 9 mm to 23 mm, and then apply a linear fit to obtain a slope of the force-ratio curve, which is tabulated in Table 4 for each supplied current. The slope of the spring force implies the spring stiffness; hence we denote this term for our electromagnetic and magnetic spring as κ_e and κ_m respectively. We can express the relationship of κ_e/κ_m in terms of I from linear fitting the plot in Figure 6 as

$$\kappa_e/\kappa_m = 4.45\times10^{-4} + 0.01773*I \qquad (3)$$

Our electromagnetic spring can provide a variable stiffness as a function of current magnitude and polarity only. The variable stiffness spring will be able to compensate a residual motion to stabilize the mirror when we incorporate this spring to the feedback control system. The effective range for the current-controlled stiffness is after the first quarter of the solenoid.

The Design of Electromagnetic Spring

Although the end application for this electromagnetic spring would be for the quantum gravimeter, our design is rather generic and can be adapted to other applications as well. In Figure 7, three of the electromagnetic springs are attached to the isolated platform where the mirror, motion sensors, and other necessary elements would be situated. Three supporting legs are the optimum number for sturdiness and complexness. Utilizing more than three legs may provide stronger support, but the feedback control system may be more complicated. From the experimental results, this configuration of 3 actuators will be able to work with the maximum load of 2 kg. The friction problem observed in this experiment can be resolved by changing the acrylic pipe to the

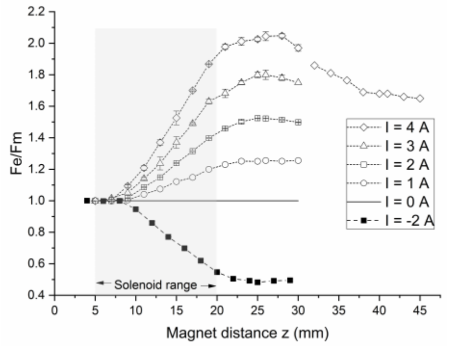

Figure 5. The force ratio F_e/F_m at different magnitude and polarity of current supplied to the solenoid. The shaded region indicates the solenoid range

Table 4. Slope of a linear fit F_e/F_m between z = 9 mm to 23 mm

I (A)	Slope of $\frac{F_e}{F_m}$ vs z : $\frac{\kappa_e}{\kappa_m}$
1	0.0182
2	0.03619
3	0.05302
4	0.0717

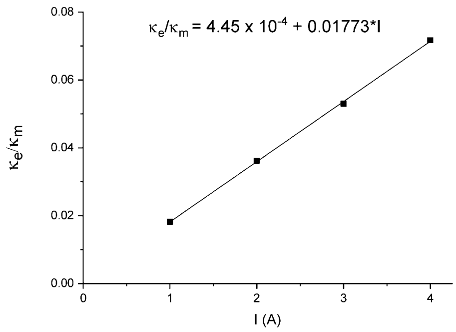

Figure 6. The stiffness ratio as a function of I

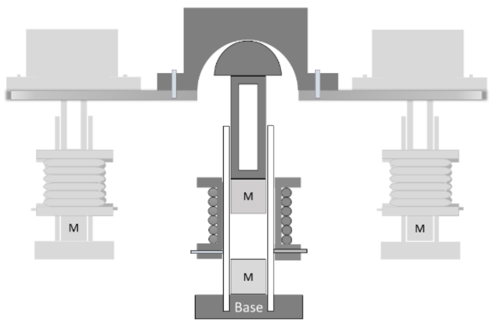

Figure 7. The design of an electromagnetic spring setup used for active vibration cancellation

aluminum tube. This design brings up the total height of approximately 10 cm. We will further incorporate this setup with the PID controller and the accelerometers to build an active vibration isolation.

Conclusions

The simplest scheme of repulsive magnetic spring inside a solenoid in which we call the electromagnetic spring is investigated for its potential use for active displacement control. The force behaviors working in the passive mode (without current) and the active mode (with the current) are characterized. In the passive mode, the stiffness of the magnetic spring increases with the magnet dimensions providing broader support and larger size. The force between the magnets as a function of the magnet separation can be well described with the multipole expansion approximation in which the small deviation may due to friction. In the active mode, the solenoid current and its polarity can modify the stiffness of the electromagnetic spring which can be used to actively compensate the unwanted movement. However, the current-controlled stiffness can only take an effect after a quarter of the solenoid range where a linear relationship of the stiffness and the current is obtained. A preliminary design of the electromagnetic spring is constructed, which is aimed for but not limited to our compact quantum gravimeter. The characterization of the force behaviors in the passive and active modes is the primary step to further design the feedback control system for active vibration isolation.

Acknowledgements

This work is part of the cooperative education program at Khon Kaen University. We would like to acknowledge financial and personnel support of the Research Center for Quantum Technology, Chiang Mai University.

References

Akshay Kumar, T. and Santhosh, B. (2021). Vibration isolation in six degrees of freedom using combined passive and active isolation technique. In: Advances in Industrial Machines and Mechanisms. Rao, Y.V.D., Amarnath, C., Regalla, S.P., Javed, A., and Singh K.K. (Eds.), p. 83-90. Springer Singapore. https://doi.org/10.1007/978-981-16-1769-0_8.

Bednarek, M., Lewandowski, D., Polczyński, K., Awrejcewicz, J., and Polczy, K. (2020). On the active damping of vibrations using electromagnetic spring. Mechanics Based Design of Structures and Machines, 49(8):1,131-1,144. https://doi.org/10.1080/15397734.2020.1819311.

Hensley, J.M., Peters, A., and Chu, S. (1999). Active low frequency vertical vibration isolation. Review of Scientific Instruments, 70(6):2,735-2,741. https://doi.org/10.1063/1.1149838.

Kasevich, M. and Chu, S. (1992). Measurement of the gravitational acceleration of an atom with a light-pulse atom interferometer. Applied Physics B Photophysics and Laser Chemistry, 54(5):321-332. https://doi.org/10.1007/BF00325375.

Olaru, R., Arcire, A., Petrescu, C., Mihai, M.M., and Gîrtan, B. (2017). A novel vibration actuator based on active magnetic spring. Sensors and Actuators, A: Physical, 264:11-17. https://doi.org/10.1016/j.sna.2017.07.041.

Otake, Y. (2000). Development of a horizontal component seismometer using a magnetic spring. Review of Scientific Instruments, 71(12):4576. https://doi.org/10.1063/1.1324735.

Oyelade, A.O. (2020). Experiment study on nonlinear oscillator containing magnetic spring with negative stiffness. International Journal of Non-Linear Mechanics, 120:103396. https://doi.org/10.1016/j.ijnonlinmec.2019.103396.

Puppin, E. and Fratello, V. (2002). Vibration isolation with magnet springs. Review of Scientific Instruments, 73(11):4,034. https://doi.org/10.1063/1.1512325.

Ravaud, R., Lemarquand, G., Babic, S., Lemarquand, V., and Akyel, C. (2010). Cylindrical magnets and coils: Fields, forces, and inductances. IEEE Transactions on Magnetics, 46(9):3585-3590. https://doi.org/10.1109/TMAG.2010.2049026.

Robertson, W., Cazzolato, B., and Zander, A. (2005). A multipole array magnetic spring. IEEE Transactions on Magnetics, 41(10):3826-3828. https://doi.org/10.1109/TMAG.2005.854981.

Schmidt, M., Senger, A., Hauth, M., Freier, C., Schkolnik, V., and Peters, A. (2011). A mobile high-precision absolute gravimeter based on atom interferometry. Gyroscopy and Navigation, 2(3):170-177. https://doi.org/10.1134/S2075108711030102.

Snamina, J. and Habel, P. (2010). Magnetic spring as the element of vibration reduction system. Mechanics and Control, 29(1), 40-44.

Sui, L., Xiong, X., and Shi, G. (2012). Piezoelectric Actuator Design and Application on Active Vibration Control. Physics Procedia, 25:1,388-1,396. https://doi.org/10.1016/j.phpro.2012.03.251.

Wu, W., Chen, X., and Shan, Y. (2014). Analysis and experiment of a vibration isolator using a novel magnetic spring with negative stiffness. Journal of Sound and Vibration, 333(13):2,958-2,970. https://doi.org/10.1016/j.jsv.2014.02.009.

Xu, J., Yang, X., Li, W., Zheng, J., Wang, Y., and Fan, M. (2020). Research on semi-active vibration isolation system based on electromagnetic spring. Mechanics and Industry, 21(1):101 https://doi.org/10.1051/meca/2019048.

Zhang, B., Dong, W., Li, X., and Long, Z. (2020). Design of active-passive composite vibration isolation system of magnetic levitation and spring based on fuzzy pid control. Proceedings - 2020 Chinese Automation Congress, CAC 2020:2,381-2,386. https://doi.org/10.1109/CAC51589.2020.9326769.